



# Tilorone increases glucose uptake in vivo and in skeletal muscle cells by enhancing Akt2/AS160 signaling and glucose transporter levels

Zoltan M. Kohler<sup>1</sup>  | Gyorgy Trencsenyi<sup>2</sup> | Laszlo Juhasz<sup>3</sup> | Agnes Zvara<sup>4</sup> | Judit P. Szabo<sup>2</sup> | Laszlo Dux<sup>1</sup> | Laszlo G. Puskas<sup>4</sup> | Laszlo Rovo<sup>5</sup> | Aniko Keller-Pinter<sup>1</sup> 

<sup>1</sup>Department of Biochemistry, Albert Szent-Gyorgyi Medical School, University of Szeged, Szeged, Hungary

<sup>2</sup>Department of Medical Imaging, Division of Nuclear Medicine and Translational Imaging, Faculty of Medicine, University of Debrecen, Debrecen, Hungary

<sup>3</sup>Institute of Surgical Research, Albert Szent-Gyorgyi Medical School, University of Szeged, Szeged, Hungary

<sup>4</sup>Laboratory of Functional Genomics, Biological Research Centre, Eotvos Lorand Research Network, Szeged, Hungary

<sup>5</sup>Department of Oto- Rhino-Laryngology and Head and Neck Surgery, University of Szeged, Szeged, Hungary

## Correspondence

Aniko Keller-Pinter, Department of Biochemistry, Albert Szent-Gyorgyi Medical School, University of Szeged, Dom Sq 9, H-6720 Szeged, Hungary.  
Email: [keller.aniko@med.u-szeged.hu](mailto:keller.aniko@med.u-szeged.hu)

## Funding information

National Research, Development and Innovation Office of Hungary; National Research, Development and Innovation Fund; János Bolyai Research Scholarship of the Hungarian Academy of Sciences; New National Excellence Program of the Ministry for Innovation and Technology Sciences; University of Szeged Open Access Fund

## Abstract

Skeletal muscle plays a major role in whole-body glucose metabolism. Insulin resistance in skeletal muscle is characterized by decreased insulin-stimulated glucose uptake resulting from impaired intracellular trafficking and decreased glucose transporter 4 (GLUT4) expression. In this study, we illustrated that tilorone, a low-molecular-weight antiviral agent, improves glucose uptake in vitro and in vivo. Tilorone increased bone morphogenetic protein (BMP) signaling in C2C12 myoblasts, the transcription of multiple BMPs (BMP2, BMP4, BMP7, and BMP14), Smad4 expression, and the phosphorylation of BMP-mediated Smad1/5/8. The activation of Akt2/AS160 (TBC1D4) signaling, the critical regulator of GLUT4 translocation, was also increased, as well as the levels of GLUT4 and GLUT1, leading to enhanced uptake of the radioactively labeled glucose analog <sup>18</sup>F-fluoro-2-deoxyglucose (<sup>18</sup>FDG). However, this excess glucose content did not result in increased ATP formation by mitochondrial respiration; both basal and ATP-linked respiration were diminished, thereby contributing to the induction of AMPK. In differentiated myotubes, AS160 phosphorylation and <sup>18</sup>FDG uptake also increased. Moreover, tilorone administration further increased insulin-stimulated phosphorylation of Akt2 and glucose uptake of myotubes indicating an insulin-sensitizing effect. Importantly, during in vivo experiments, the systemic administration of tilorone resulted in increased <sup>18</sup>FDG uptake of skeletal muscle, liver, and adipose tissue in C57BL/6 mice. Our results provide new perspectives for the treatment of type 2 diabetes, which has a limited number of treatments that regulate protein expression or translocation.

## KEYWORDS

BMP, GLUT, insulin sensitivity, mitochondria, skeletal muscle, tilorone

This is an open access article under the terms of the Creative Commons Attribution-NonCommercial-NoDerivs License, which permits use and distribution in any medium, provided the original work is properly cited, the use is non-commercial and no modifications or adaptations are made.

© 2023 The Authors. *Journal of Cellular Physiology* published by Wiley Periodicals LLC.

## 1 | INTRODUCTION

Approximately 40% of the human body is composed of skeletal muscle, which is responsible for 90% of glucose elimination after meals (DeFronzo & Tripathy, 2009). The primary glucose transporter (GLUT) in skeletal muscle and adipose tissue is GLUT4, which is responsible for insulin-stimulated glucose uptake and metabolism (Huang & Czech, 2007). GLUT4 is a member of the solute carrier family 2 (Slc2) gene family, which includes GLUT1–12 (Joost et al., 2002). Beyond GLUT4, skeletal muscle also express GLUT1 transporters. The relative amounts of GLUT4 and GLUT1 in skeletal muscles depend on the developmental stage, and GLUT1 plays a major role in glucose transport in C2C12 myoblasts (Rauch & Loughna, 2005; Zorzano et al., 2000).

When insulin binds to insulin receptors on the surface of skeletal muscle cells, activation of the phosphoinositide-3-kinase (PI3K)/protein kinase B (Akt)/Akt substrate of 160 kDa (AS160; also known as TBC1D4) pathway leads to the translocation of GLUT4-containing vesicles from the cytosol to the cell membrane and consequently glucose uptake (Leto & Saltiel, 2012). Akt regulates the Rab GTPase-activating protein (GAP) AS160, which regulates the activity of the small GTPases Rab8a, Rab13, and Rab14 in muscle cells (Ishikura et al., 2007; Sun et al., 2010). These Rab GTPases bind to static (MICAL-L2,  $\alpha$ -actinin-4, actin filaments) and motile (MyoVa) effectors that allow mobilization of the GLUT4 vesicle (Jaldin-Fincati et al., 2017). In contrast, GLUT1 is an insulin-independent transporter and constitutively localizes in the plasma membrane.

The prevalence of diabetes mellitus (DM) is increasing at an alarming rate worldwide. Over a 10-year period starting in 2009, the estimated number of people (20–79 years old) living with diabetes increased dramatically by 62% from 285 to 463 million (Saeedi et al., 2019). In addition, half of all patients with diabetes (50.1%) have not been diagnosed (Saeedi et al., 2019). Over 90% of cases of DM are type 2 DM (T2DM) (Holman et al., 2015; Zimmet et al., 2001). Insulin resistance and a lack of proper insulin secretion are the causes of T2DM, also known as non-insulin-dependent DM. Insulin resistance can be defined as impaired insulin sensitivity and glucose uptake (Reaven, 1988). The only drug that directly targets GLUT4 translocation regulatory elements to improve glucose uptake by tissues is metformin (1,1-dimethylbiguanide hydrochloride), a biguanide derivative. Metformin can increase cellular glucose uptake through AMP-activated protein kinase (AMPK) (Zhou et al., 2001), which serves as the energy sensor of the cells (Hardie et al., 2012). Insulin sensitizers, such as thiazolidinediones (TZDs), are also effective oral medications for diabetes. TZDs are agonists of the nuclear receptor peroxisome proliferator-activated receptor- $\gamma$  (PPAR $\gamma$ ) and thereby improve glucose metabolism (Kahn & McGraw, 2010; Won, 2021).

Bone morphogenetic proteins (BMPs) are cytokines of the transforming growth factor- $\beta$  family that bind to dedicated BMP receptors, which in turn phosphorylate BMP-responsive Smad1/5/8 transcription factors. Activated Smad1/5/8 forms a complex with Smad4 and then translocate into the nucleus, in which they act as

transcriptional regulators (Massagué et al., 2005). Smad1/5/8 is an important positive regulator of mature muscle fibers (Sartori et al., 2013). The role of BMPs in glucose uptake is also known. Specifically, serum BMP7 levels are decreased in type 2 diabetes models, and BMP7 enhances glucose uptake of muscle and adipose tissue through PDK1/PI3K/Akt activation and GLUT4 translocation (Chattopadhyay et al., 2017). Treatment of ob/ob mice with BMP6 leads to decreases in serum lipid and glucose levels (Pauk et al., 2019). Moreover, BMP2 and BMP6 were reported as insulin sensitizers, and BMP2 and BMP6 treatment increased glucose uptake in adipocytes by upregulating PPAR $\gamma$  and GLUT4 (Schreiber et al., 2017).

The synthetic low-molecular-weight molecule tilorone dihydrochloride (hereafter tilorone) induces BMP signaling and increases the expression of BMP2 and BMP7 in epithelial cells (Leppäranta et al., 2013). The antiviral effect of the oral drug has been known since the 1970s (Krueger & Mayer, 1970), and the drug is marketed as an antiviral agent in some countries for various viral indications, such as influenza, acute respiratory viral infection, viral hepatitis, and viral encephalitis (Ekins et al., 2018). It remains effective against several viruses at present, such as herpes simplex virus, West Nile virus, Ebola virus (Ekins et al., 2018; Katz et al., 1976; Loginova et al., 2004), and human coronaviruses including MERS-CoV (Shen et al., 2019) and SARS-CoV-2 (Puhl et al., 2021).

Because tilorone can enhance the transcription of BMPs in epithelial cells (Leppäranta et al., 2013), and BMPs might participate in insulin sensitization, glucose uptake, carbohydrate, and lipid metabolism (Schreiber et al., 2017; Yu et al., 2017), we aimed to study the effects of tilorone on signaling of myoblasts and myotubes, and for glucose uptake *in vitro* and *in vivo*. In this study, we demonstrated that tilorone induces the expression of BMPs in skeletal muscle cells and enhances the activity of BMP signaling by increasing the phosphorylation of Smad1/5/8 and expression of Smad4. The increased activation of the Akt2/AS160 pathway and the enhanced expression of GLUTs resulted in improved glucose uptake independently of insulin. Moreover, we demonstrated the insulin-sensitizing effect of tilorone by increasing insulin-mediated Akt2 phosphorylation and glucose uptake.

## 2 | MATERIALS AND METHODS

### 2.1 | Cell culture, differentiation, and treatment

Murine C2C12 myoblasts (ATCC) were grown in high-glucose Dulbecco's modified Eagle's medium (DMEM) (4.5 g/L glucose with glutamine and pyruvate; Corning) containing 20% fetal bovine serum (Gibco/Thermo Fisher Scientific) and supplemented with 50  $\mu$ g/mL gentamicin (Lonza). To induce differentiation, myoblasts were grown at 80%–90% confluency and then the medium was switched to differentiation medium containing DMEM supplemented with 2% horse serum (Sigma-Aldrich) and 50  $\mu$ g/mL gentamicin. Proliferating cells were treated with 2,7-bis[2-(diethylamino)ethoxy]-9-fluorenone dihydrochloride (tilorone dihydrochloride; #220957; Sigma-Aldrich)

at a concentration of 20 or 35 nM for 40 h. Differentiated myotubes were treated with 20 nM tilorone (2 or 5 h) followed by 100 nM insulin (Humulin-R; Eli Lilly) for 10 min on the 5th day of differentiation.

## 2.2 | Experimental animals

12 weeks old, male C57BL/6J mice ( $n = 4$ ; The Jackson Laboratory) were used for the experiments. Animals were housed under conventional conditions at  $23 \pm 2^\circ\text{C}$  with  $50 \pm 10\%$  humidity and artificial lighting with a circadian cycle of 12 h. The semisynthetic diet (VRF1; Akromon Ltd.) and drinking water were available ad libitum to all animals. The animal experiments were authorized by the Ethical Committee for Animal Research, University of Debrecen, Hungary (1/2017/DEBÁB). Laboratory animals were kept and treated in compliance with all applicable sections of the Hungarian Laws and animal welfare directions and regulations of the European Union.

## 2.3 | Quantitative real-time (qRT)-PCR

qRT-PCR was performed using a RotorGene 3000 instrument (Qiagen) with gene-specific primers and the SybrGreen protocol to monitor gene expression. One microgram of C2C12 total RNA was reverse-transcribed in a final volume of 30  $\mu\text{L}$  using a High-Capacity cDNA Archive Kit (Thermo Fisher Scientific) according to the manufacturer's instructions. The reverse transcription protocol was as follows: 10 min at room temperature, 2 h at  $37^\circ\text{C}$ , 5 min on ice, and 10 min at  $75^\circ\text{C}$  for enzyme inactivation. These steps were performed in a thermal cycler. After a twofold dilution, 1  $\mu\text{L}$  of the diluted reaction mix was used as the template for qRT-PCR. Reactions were performed with qPCRBIO SyGreen Mix Lo-ROX mix (PCR

Biosystems) according to the manufacturer's instructions at a final primer concentration of 250 nM under the following conditions: 2 min at  $95^\circ\text{C}$  followed by 40 cycles of  $95^\circ\text{C}$  for 5 s and  $60^\circ\text{C}$  for 30 s. Melting temperature analysis was performed after each reaction to check the quality of the products. Primers were designed using the online Roche Universal Probe Library Assay Design Center. The quality of the primers was verified via MS analysis by Bioneer (Daejeon). Individual threshold cycle ( $C_t$ ) values were normalized to the mean  $C_t$  values of *MmHprt* and *MmRpl27* as internal control genes. Relative gene expression levels are presented as  $2^{-\Delta\Delta C_t}$  values. Information about the genes and the primers is presented in Table 1.

## 2.4 | Immunoblotting

C2C12 cells were lysed in RIPA buffer (20 mM Tris-HCl pH 7.5, 150 mM NaCl, 1 mM  $\text{Na}_2\text{EDTA}$ , 1 mM EGTA, 1% NP-40, 1% sodium deoxycholate, 2.5 mM sodium pyrophosphate, 1 mM  $\beta$ -glycerophosphate, 1 mM  $\text{Na}_3\text{VO}_4$ , 1  $\mu\text{g}/\text{mL}$  leupeptin; #9806; Cell Signaling Technology) supplemented with 1 mM sodium fluoride and a protease inhibitor cocktail (#P8340; Sigma-Aldrich).

First, the lysates were centrifuged at  $16,000\times g$  for 5 min at  $4^\circ\text{C}$ , and then protein levels were determined using the bicinchoninic acid method (#23227; Thermo Fisher Scientific). Equal amounts of proteins were separated via sodium dodecyl sulfate-polyacrylamide gel electrophoresis and transferred to Protran nitrocellulose membrane (GE Healthcare). The membranes were blocked in tris buffered saline containing 5% skimmed milk and 0.1% Tween-20 (Sigma-Aldrich) for 1 h at room temperature. Then, the membranes were incubated at  $4^\circ\text{C}$  overnight with the following rabbit polyclonal primary antibodies: phospho-AS160 (Thr642; #8881), AS160 (#2670), PGC-1 $\alpha$  (#2178), phospho-AMPK (Thr172; #2535), AMPK (#2532), phospho-Akt2 (Ser474; #8599), Akt2 (#3063), phospho-

**TABLE 1** List of investigated genes and primers used in qRT-PCR experiments.

Reference sequence	Gene name	Description	Primers	
			Forward	Reverse
NM_007553.3	Bmp2	Bone morphogenetic protein 2	ttccatcacgaagaagccgt	ttccatcacgaagaagccgt
NM_007554.3	Bmp4	Bone morphogenetic protein 4	tctgcaggaaccaatggagc	aaaggctcagagaagctgcg
NM_007557.3	Bmp7	Bone morphogenetic protein 7	cgagacctccagatcacagt	cagcaagaagaggtccgact
NM_008109.3	GDF5 (Bmp14)	Growth differentiation factor 5, bone morphogenetic protein 14	tcctaagctctttaaggagagc	aagtcaccaggcacaaggt
NM_008540.2	Smad4	SMAD family member 4	attggatggagacttcagg	tgcttagttcattctgtgatcatc
NM_011400.3	Slc2a1 (GLUT1)	Solute carrier family 2 (facilitated glucose transporter), member 1	gatcccagcagcaagaaggt	tagccgaactgcagtgatcc
NM_001359114.1	Slc2a4 (GLUT4)	Solute carrier family 2 (facilitated glucose transporter), member 4	gctctgacgtaaggatgggg	tcaatcaccttctgtggggc
NM_013556.2	HPRT	Hypoxanthine guanine phosphoribosyl transferase	cctcctcagaccgctttt	aacctggtcatcatcgctaa
NM_011289.3	RPL27	Ribosomal protein L27	tgaaggttagcggaagtgc	tttcatgaactgccatctc

Abbreviations: BMP, bone morphogenetic protein; GLUT, glucose transporter; qRT-PCR, quantitative real-time PCR.

Smad1/5/8 (Smad1 [Ser463/465]/Smad5 [Ser463/465]/Smad9 [Ser465/467]; #13820), PPAR $\gamma$  (#2435), and GAPDH (#2118), all from Cell Signaling Technology, desmin (#M076029-2; DAKO; Agilent), GLUT1 (#PA1-46152; Thermo Fisher Scientific), or GLUT4 (#NBP1-49533; Novus Biologicals). Membranes were subsequently incubated with the horseradish peroxidase-conjugated anti-rabbit IgG secondary antibody (#P0448) from DAKO. Peroxidase activity was developed using the enhanced chemiluminescence (#K-12045 Advanta) procedure and the chemiluminescence signal was recorded using X-ray films (Agfa). On the scanned X-ray films, bands were selected with uniformed square ROIs (region of interest) using the BioRad Quantity One Analysis Software (Bio-Rad). Then, using the "Volume Analysis Report" function, we obtained the intensity of the selected area normalized to the background.

## 2.5 | Assessment of mitochondrial oxygen consumption using high-resolution respirometry

To assess respiration after 40 h of tilorone treatment, intact C2C12 myoblasts ( $3 \times 10^6$  cells) were suspended in MiRO5 respiration medium (pH 7.1; oxygen solubility factor 0.92) and gently pipetted into oxygraph chambers (Oxygraph-2k; Oroboros Instruments). All measurements were performed in 2 mL of respiration medium under continuous magnetic stirring (750 rpm) at 37°C. To avoid the effects of low O<sub>2</sub> levels on mitochondrial respiration, chamber O<sub>2</sub> concentrations were kept in the range of 50–200  $\mu$ M without reoxygenation (Doerrier et al., 2018; Nászai et al., 2019). After stable routine respiration (without exogenous substrates and ADP), ATP synthase was inhibited with oligomycin (2.5  $\mu$ M; leak respiration). The capacity of the electron transport system (ETS) was maximized via the stepwise titration of a protonophore (carbonyl cyanide *m*-chlorophenylhydrazone [CCCP]; final concentration: 0.25  $\mu$ M/step). Following complex I inhibition (with 0.5  $\mu$ M rotenone), ETS-independent respiration (or residual oxygen consumption [ROX]) was determined in the presence of the complex III inhibitor antimycin A (2.5  $\mu$ M). DatLab 7.3 software (Oroboros Instruments) was used for online display, respirometry data acquisition, and analysis.

## 2.6 | Fluorescent staining and microscopy

For anti-GLUT4 immunofluorescence, the samples were fixed with 4% paraformaldehyde (Molar Chemicals Kft.) for 15 min at room temperature, permeabilized with 0.2% Triton X100 (Sigma-Aldrich), and blocked with 2% bovine serum albumin (Sigma-Aldrich) in PBS. Rabbit polyclonal anti-GLUT4 primary antibody (#NBP1-49533; Bio-Techne) was visualized with the appropriate Alexa Fluor 488-conjugated secondary antibody (#711-545-152; Jackson ImmunoResearch).

To label the mitochondria, the cells were incubated with MitoTracker™ Deep Red FM (#M22426; Thermo Fisher Scientific) and then fixed with 4% paraformaldehyde (Molar Chemicals Kft.) for

15 min at room temperature. The nuclei were counterstained with Hoechst 33258 (#94403; Sigma-Aldrich).

Wide-field fluorescence images were obtained using a Nikon Eclipse Ni-U fluorescence microscope (Nikon Instruments Inc.) with a  $\times 100$  objective (Nikon CFI Plan Apo DM Lambda  $\times 100$  Oil, NA = 1.45). Following background correction, the images were evaluated, and heat maps were generated using ImageJ software (National Institutes of Health).

Leica DMI1 phase-contrast microscope (Leica Microsystems) with a  $\times 10$  objective (Leica Hi Plan  $\times 10$ , NA = 0.28) was used to obtain representative images demonstrating the morphology of the undifferentiated and differentiated C2C12 cells.

## 2.7 | Measurement of <sup>18</sup>F-fluoro-2-deoxyglucose (<sup>18</sup>FDG) uptake in vitro

To monitor the uptake of the radioactive glucose analog <sup>18</sup>FDG, by cells, C2C12 cells were seeded into six-well plates ( $0.08\text{--}0.1 \times 10^6$  cells/well) in 2 mL of culture medium containing 20 or 35 nM tilorone. After 24 h of culture, the monolayer surface was washed with DMEM containing 1 mM glucose and 20% FBS. To test the role of GLUT1 in glucose uptake, tilorone-treated cultures were incubated with a GLUT1 inhibitor, BAY-876 (#SML1774; Sigma-Aldrich; 10 nM, 2 h). <sup>18</sup>FDG (10  $\mu$ Ci [0.37 MBq]) in 1 mL of DMEM containing 1 mM glucose and 20% FBS was added to each well. In the samples preincubated with tilorone, the concentration of tilorone (20 or 35 nM) was maintained throughout the incubation period. The plates were incubated for 60 min at 37°C, the incubation solution was removed, and the cell surface was washed twice with 2 mL of room-temperature PBS. The cells were harvested and resuspended, and the radioactivity of the suspension was measured using a Packard Cobra-II Auto Gamma Counter device.

To measure the <sup>18</sup>FDG uptake of differentiated myotubes, C2C12 cells were seeded into six-well plates ( $1.8\text{--}2 \times 10^5$  cells/well) for 24 h in growth medium, and then, differentiation was induced by shifting the cells into differentiation medium containing 2% horse serum (Sigma-Aldrich). On the 5th day on differentiation, cell cultures were treated with 20 nM tilorone for 2 or 5 h and 100 nm insulin for 10 min (Humulin-R; Eli Lilly). Then, <sup>18</sup>FDG uptake was measured as described previously.

## 2.8 | Animal treatment and in vivo imaging

C57BL/6 mice were injected intraperitoneally with 25 mg tilorone/kg body weight. The treatment was repeated 3 days after the first injection and PET/CT scans were performed on the day after the second tilorone injection.

Mice were anaesthetized with 3% Forane using a dedicated small animal anesthesia device and were injected with  $10.2 \pm 0.9$  MBq of <sup>18</sup>FDG in 100  $\mu$ L saline via the lateral tail vein before and after the

second tilorone treatment. 50 min after radiotracer injection, whole-body PET/CT scans were performed in isoflurane anesthesia using the preclinical *nanoScan PET/CT* device (Mediso LTD). After the image reconstruction and PET image analysis, the standardized uptake value (SUV) was calculated using the following formula:  $SUV = (ROI \text{ activity [MBq/mL]}) / (\text{injected activity [MBq]} / \text{animal weight [g]})$  (Kocsis et al., 2014).

## 2.9 | Statistical analysis

Statistical significance between groups was analyzed via Student's *t*-test or one-way analysis of variance followed by Dunnett's post hoc test. GraphPad Prism 8.0 (GraphPad Software Inc.) was used for graphing and statistical analyses. The data are expressed as the mean + SEM or the median (horizontal line in the box) with the 25th (lower whisker) and 75th (upper whisker) percentiles are plotted on box plots.  $p < 0.05$  denoted statistical significance.

## 3 | RESULTS

### 3.1 | Tilorone increases BMP signaling in myoblasts

Leppäranta et al. (2013) demonstrated the ability of tilorone to enhance the transcription of BMP2 and BMP7 in mouse epithelial cells. Thus, we first examined whether this effect could be induced in mouse myoblasts. The treatment time we chose was based on Leppäranta's experiment, 24 and 48 h, which

were effective (Leppäranta et al., 2013). qRT-PCR revealed that mRNA levels of BMP2, BMP4, BMP7, and BMP14 were elevated by both (20 and 35 nM) concentrations in myoblasts; however, BMP14 expression was only significantly increased by the higher concentration (Figure 1). Moreover, the transcription of Smad4, a component of the BMP signaling pathway, was significantly increased by both concentrations (Figure 1). Further, we found that tilorone treatment increased the phosphorylation of Smad1/5/8 (Figure 2a,b), indicating the enhancement of BMP signaling.

### 3.2 | Effect of tilorone on signaling molecules regulating GLUT4 translocation

Because the transcription of several BMPs and Smad4 and phosphorylation of Smad1/5/8 were enhanced by tilorone treatment, we also examined whether these proteins affect insulin-dependent glucose uptake and assessed its regulation. BMP2 and BMP6 can sensitize adipocytes to insulin and enhance glucose uptake (Schreiber et al., 2017). The C2C12 mouse skeletal muscle cell line is a well-documented and in vitro used model for studying glucose homeostasis, insulin signaling mechanism, insulin resistance, GLUTs at the cellular and molecular levels (Mangnall et al., 1993; Tulipano et al., 2008; Wong et al., 2020). Moreover, GLUT4 translocation was also demonstrated in C2C12 myoblasts (Duan et al., 2017). We tested the expression and phosphorylation of skeletal muscle-specific Akt2, AMPK, and AS160, which regulate the insulin-dependent translocation of GLUT4. Tilorone increased the phospho-Akt2 (Ser474)/Akt2 and phospho-AMPK (Thr172)/AMPK ratios, and

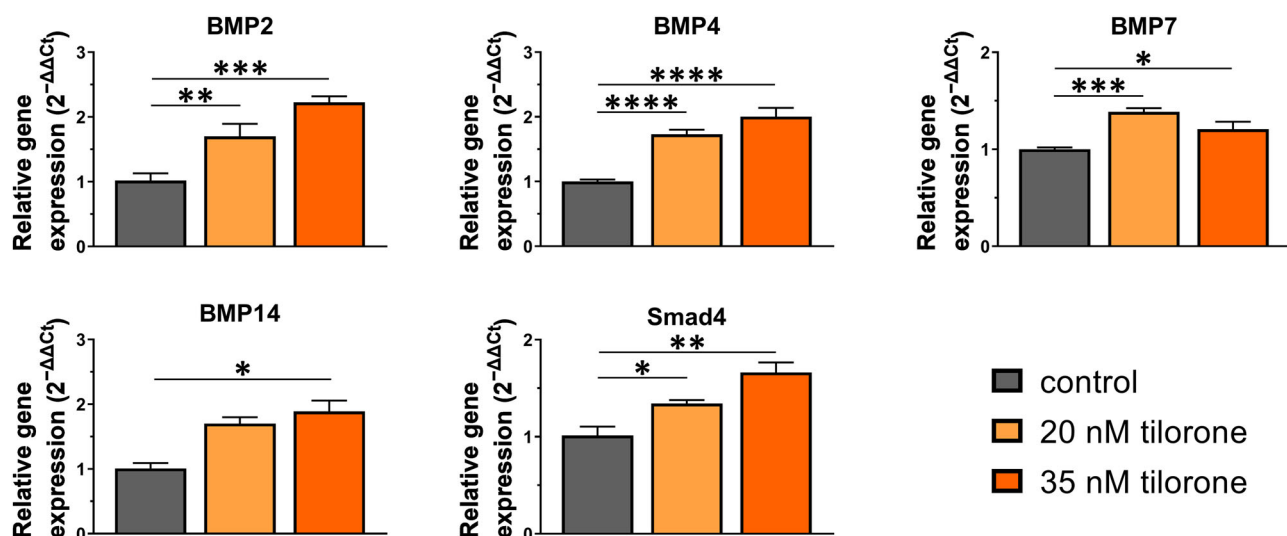


**FIGURE 1** Tilorone increases bone morphogenetic protein (BMP) and Smad4 expression in myoblasts. C2C12 myoblasts were treated with 20 or 35 nM tilorone for 40 h, and the gene expression of BMP2, BMP4, BMP7, BMP14, and Smad4 molecules was measured by quantitative real-time PCR. Relative gene expression levels as  $2^{-\Delta\Delta C_t}$  values using *MmHprt* and *MmRpl27* as internal control genes, are presented. Data are reported as the mean + SEM ( $n = 3-4$ ). \* $p < 0.05$ , \*\* $p < 0.01$ , \*\*\* $p < 0.001$ , \*\*\*\* $p < 0.0001$ . BMP, bone morphogenetic protein.

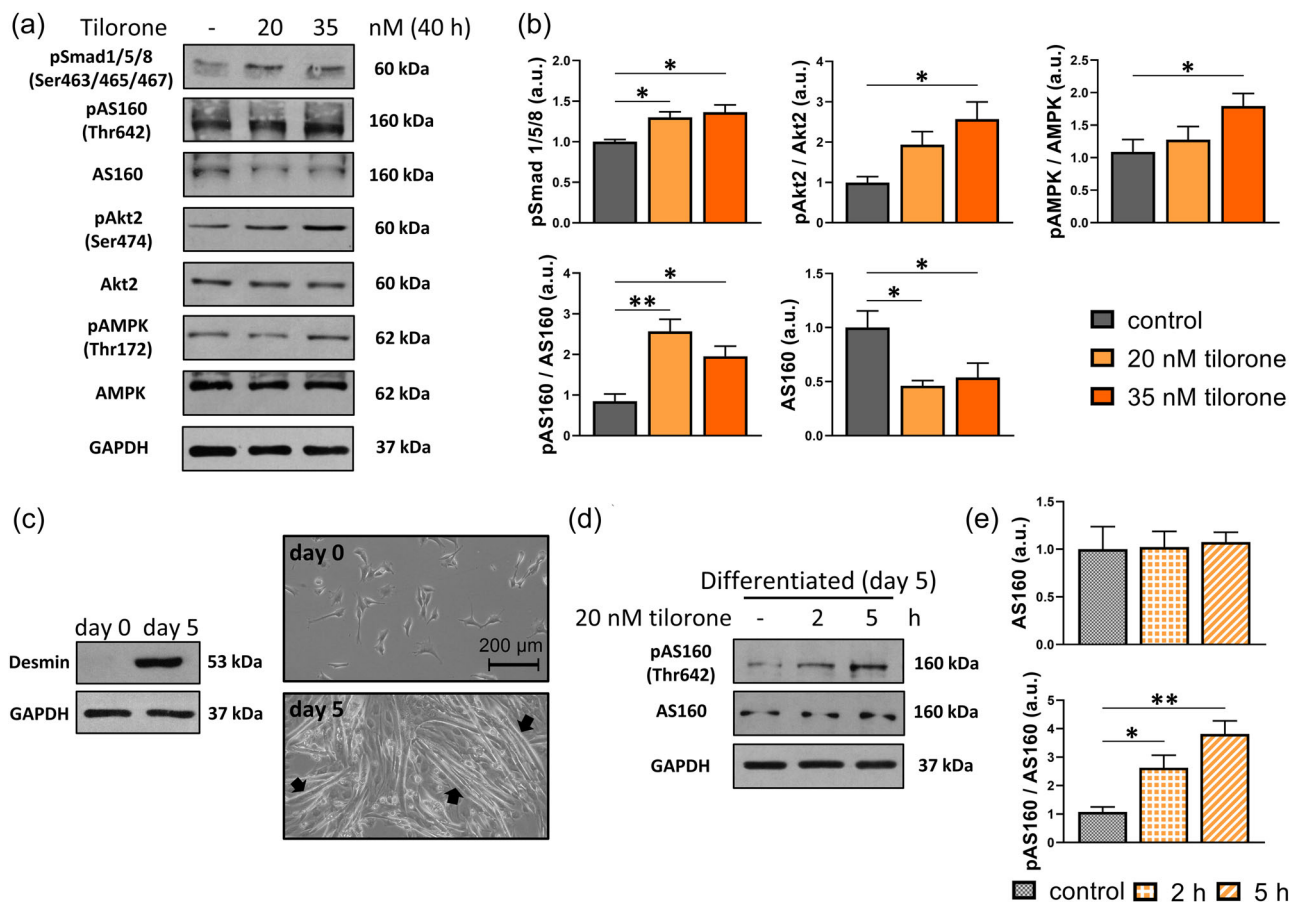


**FIGURE 2** Effect of tilorone treatment on the activity of signaling molecules. Activation of bone morphogenetic protein (BMP) pathway was represented by phospho-Smad1/5/8 (Ser463/Ser456/Ser467) levels, and the activation of the signaling pathway (protein kinase B [Akt2]), AS160 regulating glucose transporter 4 (GLUT4) translocation was also studied. (a) Representative Western blots depict the levels of phospho-Smad1/5/8 (Ser463/Ser456/Ser467), phospho-AS160 (Thr642), AS160, phospho-Akt2 (Ser474), Akt2, phospho-AMPK(Thr172), and AMPK in proliferating C2C12 cells following 40 h tilorone treatment. GAPDH was used as a loading control. (b) Quantification of the Western blot results normalized to control and reported as the mean + SEM ( $n = 3-8$  independent experiments). (c) Representative phase-contrast images of undifferentiated (proliferating) and differentiated C2C12 cells at  $\times 10$  magnifications. Arrows mark the myotubes. Representative immunoblot shows the expression levels of desmin in undifferentiated (Day 0) and differentiated (Day 5) C2C12 cells. GAPDH was used as the loading control. (d) Representative Western blots depict the phospho- and total AS160 levels in differentiated C2C12 myotubes after 2 or 5 h of 20 nM tilorone treatment. GAPDH was used as a loading control. (e) For quantifying the western blot results, data were normalized to the control and reported as mean + SEM ( $n = 3$  independent experiments).  $*p < 0.05$ ,  $**p < 0.01$ . AMPK, AMP-activated protein kinase; au, arbitrary unit.

these changes were significant for 35 nM tilorone. AS160 expression was decreased by both tilorone concentrations, and the phospho-AS160/AS160 ratio was increased (Figure 2a,b).

Subsequently, myoblasts were differentiated into myotubes in vitro (Figure 2c). To monitor the process of myoblast differentiation, we evaluated the amount of desmin, a muscle-specific intermediate filament. The level of desmin increased, indicating the appropriate differentiation of the samples. The levels and phosphorylation of AS160, the key regulator of GLUT4 translocation, were also examined on the fifth day of differentiation. Because tilorone affects myoblast differentiation as well (our unpublished data); therefore, we applied tilorone only for a short treatment in differentiated samples. In myotubes, 20 nM tilorone increased the phospho-AS160/AS160 ratio after either 2 or 5 h treatment (Figure 2d,e).

### 3.3 | Tilorone increases the expression of GLUTs and glucose uptake of C2C12 cells

Because the increased phosphorylation of Akt2, AMPK, and AS160 favors GLUT4 translocation and glucose uptake, we next studied the intracellular expression of GLUT4 in myoblasts exposed to tilorone via immunofluorescence staining and wide-field fluorescent microscopy. In addition to the original representative images, pseudocolor images provide better visualization of the altered GLUT4 expression depicting the increased levels of GLUT4 fluorescence following tilorone treatment (Figure 3a). The high-intensity red and yellow areas were mainly adjacent to the nucleus in tilorone-treated cells (Figure 3a). Quantification of the whole GLUT4 fluorescence intensity of the cells illustrated that their GLUT4 content increased after tilorone treatment (Figure 3b).

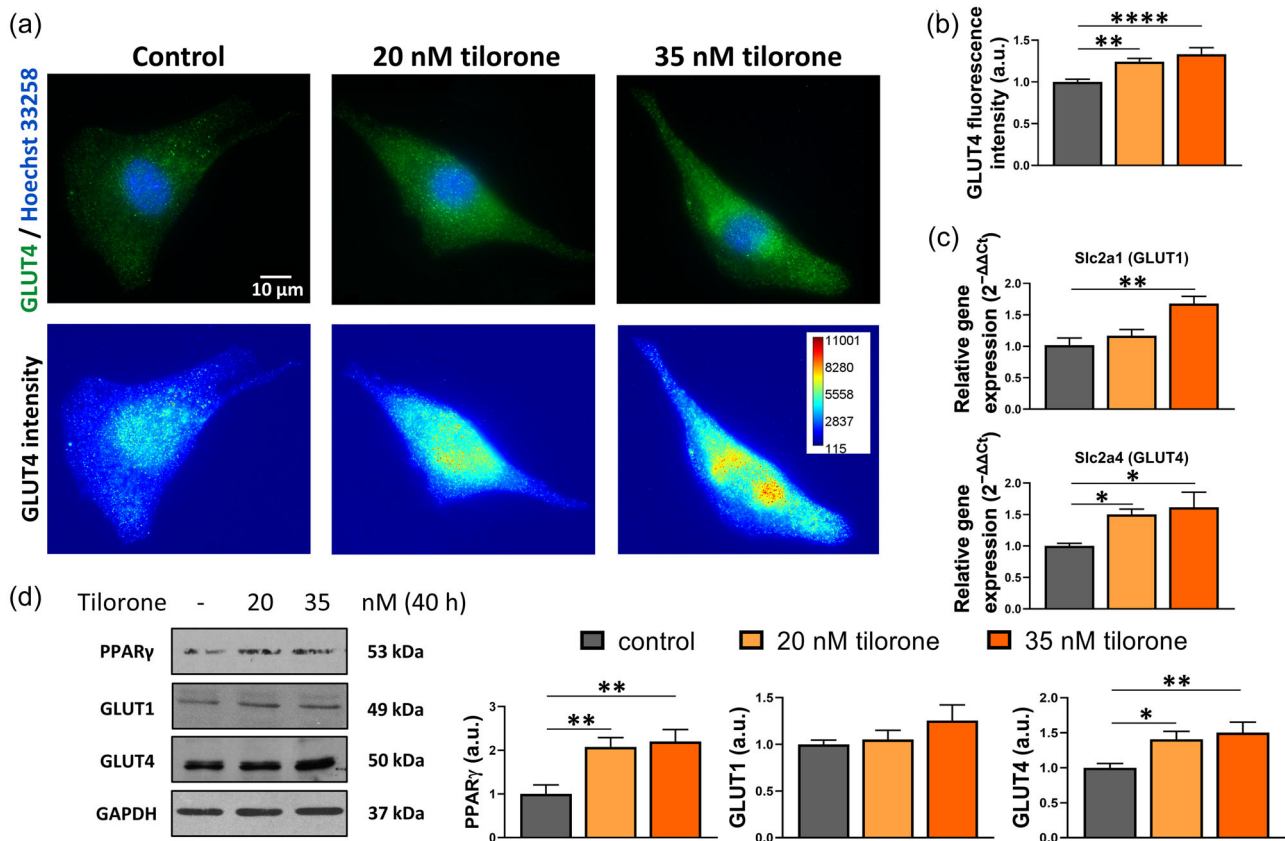


**FIGURE 3** Tilorone increases the expression of glucose transporters (GLUTs). (a) Representative wide-field fluorescence images reveal the distribution of GLUT4 following staining with Alexa Fluor 488 (green). Nuclei were stained by Hoechst 33258 (blue). Representative pseudocolor images depict the GLUT4 signal intensity. The color was assigned to each pixel based on the pixel intensity value according to the calibration bar. (b) The mean intensity values of the cells were quantified, normalized to control, and compared following tilorone treatment. Data are reported as the mean + SEM ( $n = 3$  independent experiments, 36–41 cells/treatment were quantified). (c) The levels of *Slc2a1* (GLUT1) and *Slc2a4* (GLUT4) were studied by quantitative real-time PCR. The housekeeping genes *MmHprt* and *MmRpl27* were used as internal controls to normalize qRT-PCR results, and relative gene expression levels were calculated using the  $2^{-\Delta\Delta C_t}$  method. Data are reported as the mean + SEM ( $n = 3$ –4 independent experiments). (d) Representative western blots of PPAR $\gamma$ , GLUT1, and GLUT4 protein expression. GAPDH was used as an internal control. Quantification of the results normalized to control and reported as the mean + SEM (GLUT1:  $n = 3$ , PPAR $\gamma$  and GLUT4:  $n = 8$  independent experiments). \* $p < 0.05$ , \*\* $p < 0.01$ , \*\*\*\* $p < 0.0001$ . au, arbitrary unit; PPAR $\gamma$ , peroxisome proliferator-activated receptor- $\gamma$ .

Subsequently, qRT-PCR was performed to check the mRNA levels of myoblast-specific *Slc2a1* (GLUT1) and *Slc2a4* (GLUT4). We found that the levels of both the *Slc2a1* and *Slc2a4* transcripts were increased by treatment with different concentrations of tilorone (Figure 3c). GLUT1 and GLUT4 protein levels were also analyzed by Western blot. GLUT1 levels were tendentially increased following tilorone treatment, and we detected a significant increase in GLUT4 protein levels at 35 nM tilorone concentration (Figure 3d). From the research of Schreiber et al. (2017) using mouse adipocytes, we know that *Smad1/5/8* and *Smad4* can transcriptionally activate PPAR $\gamma$ , which is a critical regulator of GLUT4 expression. We thus examined the expression of PPAR $\gamma$  by Western blot technique and detected an increase in both tilorone concentrations (Figure 3d).

Because we observed increased levels of GLUTs and strong activation of Akt2/AS160 signaling that regulate GLUT4 translocation, radiolabeled glucose analog  $^{18}\text{F}$ FDG uptake of C2C12 cells was also measured. Our results revealed a 1.5-fold increase in  $^{18}\text{F}$ FDG

uptake after 20 nM tilorone treatment, and this uptake was further increased by the higher concentration (Figure 4a). To separate the rate of glucose uptake via GLUT1 or GLUT4, we applied BAY-876, a GLUT1-specific inhibitor to the cells after preincubation with tilorone. BAY-876 treatment decreased the  $^{18}\text{F}$ FDG uptake of the cells indicating the involvement of GLUT1 in tilorone-mediated glucose uptake (Figure 4b).

### 3.4 | Tilorone increases $^{18}\text{F}$ FDG uptake of myotubes and enhances insulin effect

Because tilorone increased glucose uptake in myoblasts, next we examined whether tilorone exhibits an insulin sensitizing effect on myotubes. The phosphorylation of Akt2, a critical element of insulin-mediated signaling, was significantly increased following insulin treatment, as expected (Figure 5a,b). Administration of

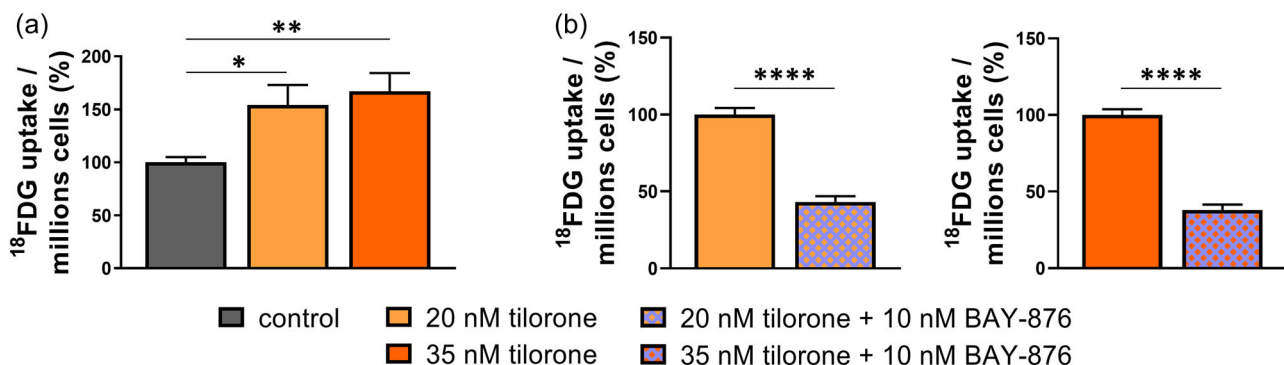


**FIGURE 4** Tilorone increases <sup>18</sup>F-fluoro-2-deoxyglucose (<sup>18</sup>FDG) uptake by C2C12 cells. (a) Rate of uptake of the radioactively labeled glucose analog <sup>18</sup>FDG by C2C12 myoblasts following 20 or 35 nM tilorone treatment (24 h). <sup>18</sup>FDG uptake is expressed as percentage of 1 × 10<sup>6</sup> myoblasts relative to the control. (b) The effect of BAY-876 (2 h, 10 nM), a GLUT1 inhibitor, on <sup>18</sup>FDG uptake of tilorone-treated (24 h; 20 or 35 nM) C2C12 myoblasts. <sup>18</sup>FDG uptake is expressed as percentage of 1 × 10<sup>6</sup> myoblasts relative to tilorone treated cells. Results are reported as the mean + SEM (n = 5–7 independent experiments). \*p < 0.05, \*\*p < 0.01, \*\*\*\*p < 0.0001. GLUT, glucose transporter.

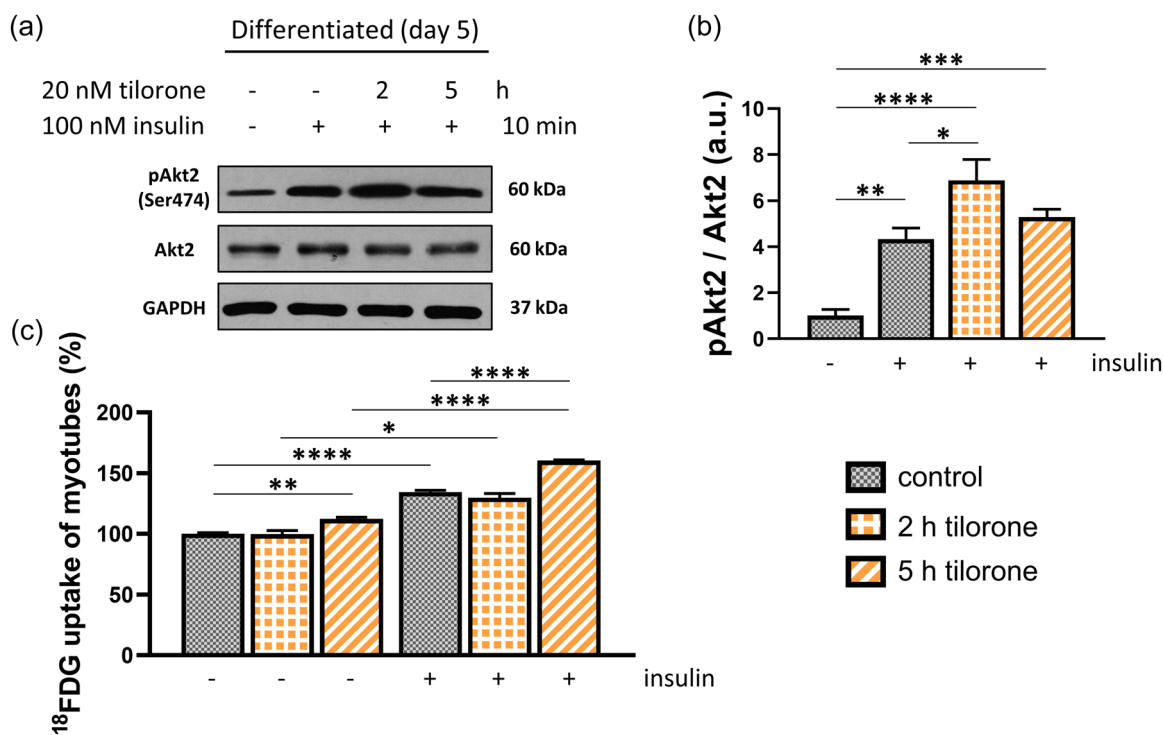


**FIGURE 5** Tilorone increases insulin effect and improves <sup>18</sup>FDG uptake in myotubes. (a) Representative Western blots depict the levels of phospho-Akt2 (Ser474), Akt2, and GAPDH in differentiated C2C12 myotubes after tilorone pretreatment (20 nM, 2 or 5 h) followed by insulin administration (100 nM, 10 min). GAPDH shows the equal loading of samples. (b) Quantification of the western blot results, data normalized to untreated control and reported as the mean + SEM (n = 3–4 independent experiments); \*p < 0.05, \*\*p < 0.01, \*\*\*\*p < 0.0001. (c) The radioactively labeled glucose analog <sup>18</sup>FDG uptake of C2C12 myotubes following 20 nM tilorone (2 or 5 h) administration and with or without insulin (10 min 100 nM) treatment. <sup>18</sup>FDG uptake is expressed as a percentage of the untreated control group. Results are reported as the mean + SEM (n = 4 independent experiments); \*p < 0.05, \*\*p < 0.01, \*\*\*\*p < 0.0001.

tilorone further increased the insulin-induced phospho-Akt2/ Akt2 indicating the insulin-sensitizer effect of tilorone (Figure 5a,b).

Next, we examined the <sup>18</sup>FDG uptake of myotubes on the fifth day of differentiation. We observed increased <sup>18</sup>FDG uptake

of myotubes after tilorone treatment (5 h). Insulin increased the <sup>18</sup>FDG uptake of control and tilorone-treated (2 or 5 h tilorone administration) groups. Moreover, tilorone administration (5 h) increased the insulin-mediated <sup>18</sup>FDG uptake of myotubes (Figure 5c).



### 3.5 | Effects of tilorone treatment on mitochondrial function in myoblasts

To determine whether the elevated glucose uptake of the cells was associated with changes in the mitochondrial respiratory chain, the oxygen consumption of C2C12 cells was examined via high-resolution respirometry. Routine (baseline), proton leak, ETS (representing maximal respiration capacity), and ROX values are presented in a representative measurement plot in Figure 6a. Compared to the control group findings, treatment with 20 or 35 nM tilorone significantly decreased routine respiration in intact myoblasts. In addition, tilorone reduced ATP-linked respiration (difference between routine and leak respiration) based on the unchanged leak values (Figure 6b). Following oligomycin treatment, the oxygen consumption represents the level of proton leak in the cells. No significant difference in the maximal capacity of ETS and ROX was observed following treatment. Mitochondrial reserve capacity (respiration reserve), the difference between the respiratory capacity and basal respiration, is the “spare” respiratory capacity important for cellular responses to stress and preventing oxidant-induced mitochondrial dysfunction (Dranka et al., 2010). In our experiments, the mitochondrial reserve capacity did not change after tilorone administration.

As we observed changes of mitochondrial function, we next studied the expression of PPAR $\gamma$  coactivator 1 alpha (PGC-1 $\alpha$ ) which regulates mitochondrial biogenesis, and total number of mitochondria in the cells was also evaluated. The PGC-1 $\alpha$  protein levels did not change following either 20 or 35 nM tilorone treatment (Figure 6c) analyzed by western blot. To achieve total number of mitochondria in the cells, we visualized mitochondria using the specific fluorescent dye MitoTracker™ Deep Red FM, which passively diffuses across the plasma membrane of living cells and accumulates in active mitochondria (Figure 6d). We measured the total fluorescent intensity of the cells and found no difference between control and tilorone-treated cells (Figure 6e), indicating that the mitochondrial number did not change following tilorone treatment.

### 3.6 | Tilorone administration increases <sup>18</sup>FDG uptake in vivo

Considering the increased glucose uptake of skeletal muscle myoblasts in vitro, we next examined the effect of systemic tilorone administration on in vivo <sup>18</sup>FDG uptake using PET/CT imaging. The treatment concentration we chose was based on earlier in vivo experiments and pharmacokinetics evaluation of tilorone (Leppäranta et al., 2013). The distribution of radiolabelled glucose in C57BL/6 mice was examined by PET/CT scans (Figure 7a). By the quantitative analysis <sup>18</sup>FDG-PET images, we found significant increases in the SUV mean of skeletal muscle, adipose tissue, and liver following tilorone treatment, indicating the increased radiotracer uptake of these tissues. The <sup>18</sup>FDG accumulation was comparable in tilorone treated skeletal muscle, adipose tissues, and liver (Figure 7b). Among

the examined tissues, heart exhibited the highest basal glucose uptake; however, it did not increase after tilorone treatment (Figure 7b).

## 4 | DISCUSSION

The synthetic small-molecule compound tilorone can enhance the transcription of BMPs in epithelial cells (Leppäranta et al., 2013). BMPs might participate in insulin sensitization, glucose uptake, carbohydrate and lipid metabolism, and the regulation of mitochondrial function (Schreiber et al., 2017; Yu et al., 2017); therefore, we examined the effects of tilorone on glucose uptake and metabolism in vitro and in vivo. As the number of people with T2DM is continuously increasing, there is an urgent need for new therapeutic strategies and to identify new drug candidates that increase glucose uptake.

Tilorone first was used as a broad-spectrum antiviral agent in the 1970s. The mechanism through which tilorone mediates its effect is not completely understood. Tilorone is able to induce transcriptional changes (Ratan et al., 2008); and a possible explanation of the mechanism of its action is that tilorone can intercalate into DNA thereby affecting the expression of genes (Nishimura et al., 2007). Earlier a high-throughput drug screen identified tilorone as a BMP-inducing agent. Tilorone was shown to induce BMP genes and the expression of the BMP target gene Id3 (inhibitor of differentiation-3) in pulmonary epithelial cells in vitro, and to increase Smad1 phosphorylation in vivo (Leppäranta et al., 2013). In the muscles of tumor-bearing mice, it was also proved that tilorone effect is dependent on the BMP-Smad1/5/8 signaling pathway (Sartori et al., 2021). However, this does not exclude other possible target genes for tilorone.

In epithelial cells, tilorone has been found to increase the transcription of BMP2 and BMP7, but not BMP4 (Leppäranta et al., 2013). We observed increased BMP2, BMP4, BMP7, and BMP14 transcription in C2C12 myoblasts following tilorone administration. Moreover, we observed increased Smad1/5/8 phosphorylation and increased Smad4 transcription following tilorone treatment, indicating the enhanced BMP signaling. Several studies investigated the effect of tilorone on different cell types. In this study, we used a tilorone concentration comparable to the antiviral concentration of tilorone (Lane & Ekins, 2020).

Tilorone possesses a broad array of biological activities beyond its antiviral effect. In addition to alleviating pulmonary fibrosis in a mouse model (Leppäranta et al., 2013), a recent publication demonstrated that tilorone represents a potential novel therapy for fibrosis associated with heart failure (Horlock et al., 2021), and can also prevent muscle wasting and preserve the function of neuromuscular junction of tumor-bearing mice (Sartori et al., 2021). Since the Smad1/5/8-mediated BMP signaling was identified as an important regulator of muscle homeostasis affecting skeletal muscle size or the function of neuromuscular junction, the potential therapeutic application of tilorone in muscle wasting diseases of different origin might be an interesting perspective.

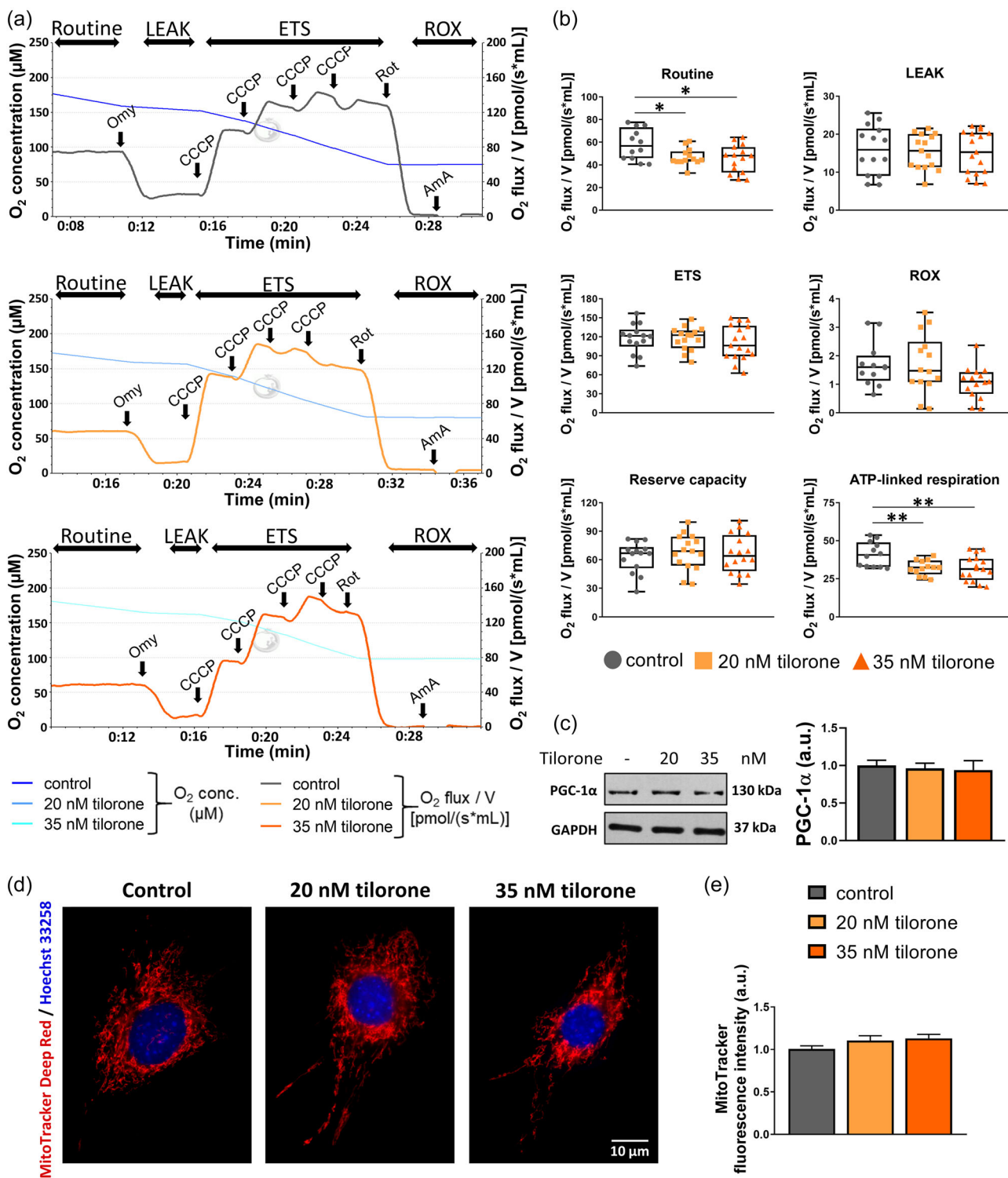


**FIGURE 6** Changes in mitochondrial respiration in C2C12 myoblasts after tilorone treatment. (a) On the representative experimental figures of the mitochondrial respiration measurements, the lines illustrate chamber O<sub>2</sub> concentrations in control and tilorone-treated cells. Maximal electron transport system (ETS) capacity was achieved via stepwise titration of an uncoupler (carbonyl cyanide m-chlorophenylhydrazone [CCCP]). (b) Measured routine respiration, leak state, maximal ETS capacity, residual oxygen consumption (ROX), reserve capacity, and ATP-linked respiration are presented as O<sub>2</sub> flux/V (pmol/[s × mL]). The box plots demonstrate the median (horizontal line in the box) and the 25th (lower whisker) and 75th (upper whisker) percentiles (n = 12–17 independent experiments). (c) Illustrative western blot image of PGC-1α expression and GAPDH as a loading control. To quantify the results, the data were normalized to the control and then the mean + SEM was plotted (n = 5 independent experiments). (d) Representative images depict mitochondria labeled with MitoTracker Deep Red FM (red). Nuclei were stained by Hoechst 33258 (blue). (e) The fluorescence signal intensity of MitoTracker Deep Red FM staining was measured in the individual cells, and the total intensity values of the cells were compared. The results were normalized to control and reported as the mean + SEM (n = 3–4 independent experiments, 49–65 cells/treatment). \*p < 0.05, \*\*p < 0.01. AmA, antimycin A; au, arbitrary unit; Omy, oligomycin; Rot, rotenone.

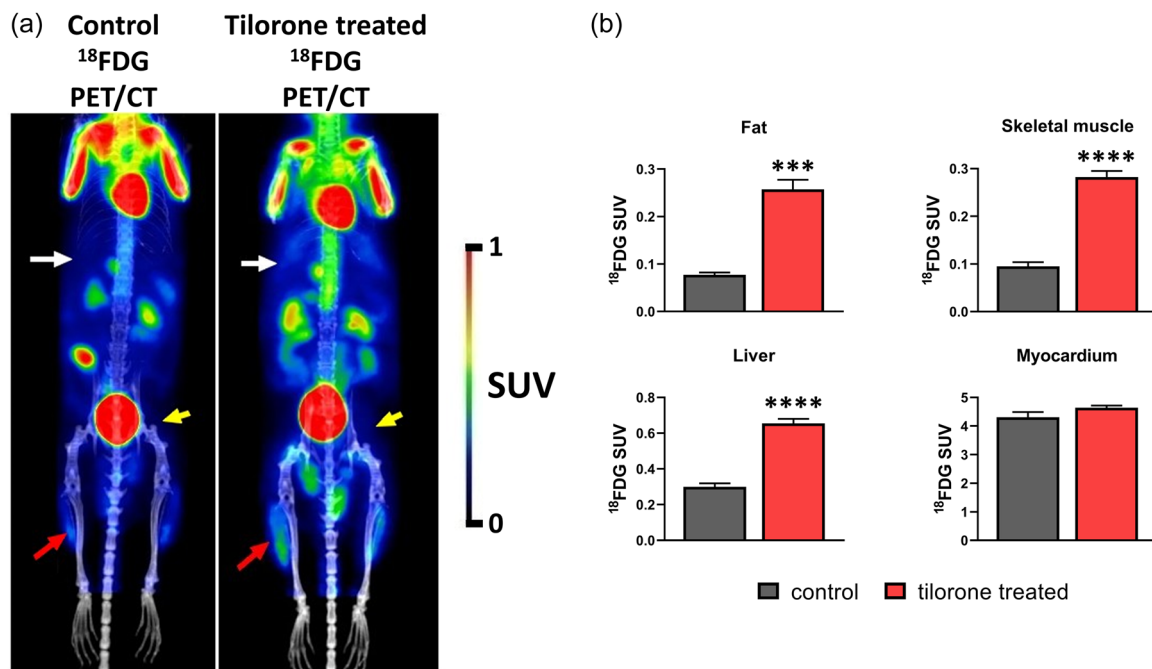


**FIGURE 7** In vivo  $^{18}\text{F}$ -fluoro-2-deoxyglucose ( $^{18}\text{F}$ FDG) uptake in C57BL/6 mice after tilorone treatment. (a) Representative decay-corrected  $^{18}\text{F}$ FDG-PET/CT MIP (maximum intensity projection) images of the same C57BL/6 mouse before (left panel) and after (right panel) tilorone treatment (25 mg/kg). White arrows: liver, yellow arrows: fat, red arrows: muscle. (b) Quantitative analysis of  $^{18}\text{F}$ FDG uptake of selected tissues (fat, liver, skeletal muscle, myocardium). Results are reported as the mean of standardized uptake value (SUV) + SEM ( $n = 4$  in each group); \*\*\* $p < 0.001$ , \*\*\*\* $p < 0.0001$ .

In our experiments, tilorone increased PPAR $\gamma$  level. In considering the transcription-regulatory effects of Smad1/5/8 and Smad4, it is important to mention their ability to control PPAR $\gamma$  (Schreiber et al., 2017). PPAR $\gamma$  can regulate cell differentiation, glucose and lipid metabolism, lipid storage and mobilization (Janani & Ranjitha Kumari, 2015), and mitochondrial biogenesis with PGC-1 $\alpha$  (Jamwal et al., 2020). Via another pathway, BMP14 can activate Sirt1, which deacetylates and thus activates PPAR $\gamma$  (D. Wang, Jiang et al., 2018). All of the BMPs we examined (i.e., BMP2, BMP4, BMP7, and BMP14) can positively regulate PPAR $\gamma$ . Several targets of active PPAR $\gamma$  include the Slc2a4 (GLUT4) gene (Armoni et al., 2007; Wu et al., 1998). Importantly, PPAR $\gamma$  agonists have emerged as effective insulin sensitizers in the treatment of type 2 diabetes. Here we observed, that tilorone exhibits an insulin-sensitizer effect increasing insulin-mediated Akt2 phosphorylation and  $^{18}\text{F}$ FDG uptake of myotubes.

Importantly, we observed that tilorone treatment affects both insulin-dependent (via GLUT4 translocation) and insulin-independent (via GLUT1) glucose uptake of myoblasts. Both the increased GLUT4 levels and activated Akt2/AS160 signaling can lead to increased GLUT4-mediated glucose uptake after tilorone treatment (summarized in Figure 8). The specific inhibition of GLUT1 markedly decreased (more than 50% inhibition) the  $^{18}\text{F}$ FDG uptake of tilorone treated cells indicating the involvement of GLUT1 in glucose uptake. The increased GLUT1 levels might participate in this effect. GLUT1 is an insulin-independent transporter, and thus, it is essentially released into the plasma membrane of cells. The presence of GLUT1 in skeletal muscle was previously reported as the predominant GLUT

isoform in myoblasts (Zhao & Keating, 2007). It was reported earlier that BMP7 augmented glucose uptake in adipose tissue and muscle by increasing GLUT4 translocation to the plasma membrane via the PI3K/PDK1/Akt pathway (Chattopadhyay et al., 2017). Consistent with the aforementioned effect, the tilorone-mediated increase of BMP transcription was associated with increased GLUT4 levels and increased activity of the signaling pathway responsible for GLUT4 translocation in our experiments. However, it is important to note, that we do not conducted the evaluation of GLUT4 specifically at the plasma membrane. Since C2C12 cells are weak models for studying GLUT4 translocation, this is a limitation of the model system.

Akt2/AS160 signaling is a central regulator of GLUT4 translocation. The pAS160/AS160 ratio increased in both myoblasts and myotubes following tilorone treatment. However, the total AS160 level was decreased in myoblasts after tilorone administration but not in myotubes. Importantly, in myoblasts we applied tilorone for 40 h; therefore, the decreased level of total AS160 protein can be the consequence of a negative feedback effect following increased glucose uptake. The 40 h tilorone treatment of myoblasts already allowed a sufficiently long period for quantitative protein changes; however, few hours (2 or 5 h) treatment on myotubes only gave the opportunity for faster phosphorylation changes.

Skeletal muscle is one of the most energy-intensive tissues in the human body. The transcription factor PGC-1 $\alpha$  plays a central role in the regulation of cellular energy metabolism by maintaining mitochondrial biogenesis and oxidative metabolism (Liang & Ward, 2006). According to our results, the number of active

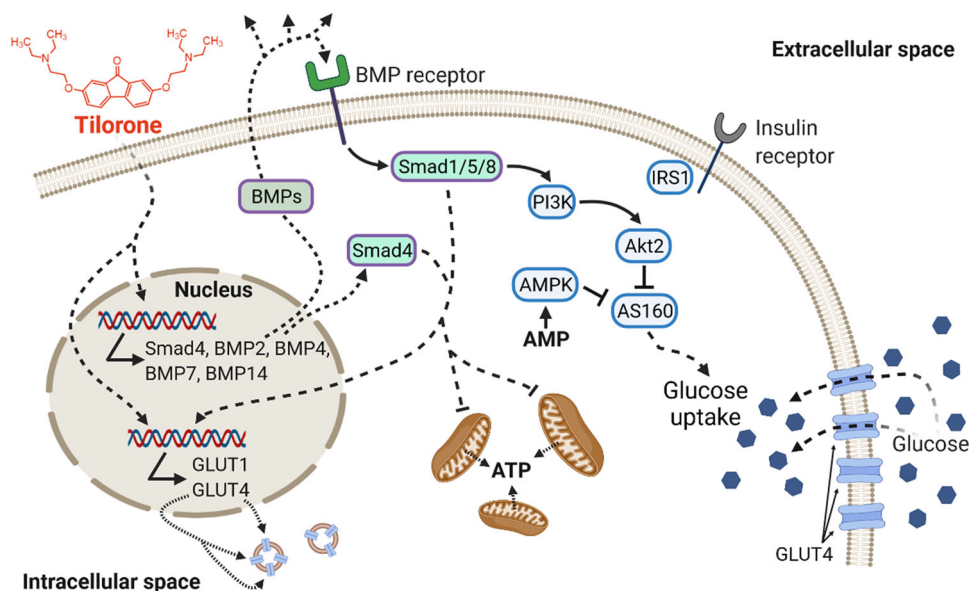


**FIGURE 8** Schematic summary of the effects of tilorone on signaling pathways and glucose uptake. Tilorone induces the transcription of BMP2, BMP4, BMP7, and BMP14, and enhances the activity of the BMP pathway by increasing the phosphorylation of Smad1/5/8 and expression of Smad4. The increased glucose transporter (GLUT1 and GLUT4) levels and activation of the Akt2/AS160 pathway can participate in increased glucose uptake. The decreased mitochondrial routine and ATP-linked respiration also favors increased glucose uptake. The figure was created using [BioRender.com](#). Akt, protein kinase B; AMP, adenosine monophosphate; AMPK, AMP-activated protein kinase; AS160, Akt substrate of 160 kDa; ATP, adenosine triphosphate; BMP, bone morphogenetic proteins; GLUT, glucose transporter; IRS1, insulin receptor substrate 1; PI3K, phosphoinositide-3-kinase.

mitochondria did not change after tilorone treatment; however, the routine and ATP-linked respiration values were decreased despite the increased glucose uptake of the cells. Therefore, decreased mitochondrial function might explain the increased glucose uptake. It cannot be ignored that tilorone has other cellular effects in addition to inducing BMPs. Together, these effects might decrease ATP-linked respiration in mitochondria, and this presumably results in an increased intracellular AMP/ATP ratio. High levels of AMP inhibit AS160 through AMPK and thereby activate GLUT4 translocation (Huang & Czech, 2007).

Several studies investigated the role of BMPs in mitochondrial function and their effect on mitochondrial number in different tissues. In brown preadipocytes, BMP4 treatment decreased PGC-1 $\alpha$  mRNA levels, whereas increased PPAR $\gamma$ 1 transcription (Modica et al., 2016). Consistent with this, the transcription of PGC-1 $\alpha$  was decreased in the brown adipose tissue of BMP-4 overexpressing transgenic mice without a change in the number of mitochondria, but the transcription of these genes was increased in white adipose tissue (Qian et al., 2013). Based on these findings, BMP4 plays a role in mitochondrial functions, albeit in a strongly tissue-specific manner. According to a study of brown adipose tissue, BMP7 can increase mitochondrial activity without increasing the number of mitochondria (Townsend et al., 2013). Increased mitochondrial oxygen consumption was also detected after BMP2 treatment in human chondrocytes (C. Wang, Silverman et al., 2018). Our results are partly consistent with these data; however, it is important to remember that we examined the effect of tilorone treatment.

In summary, this study demonstrated the complex mechanism of tilorone action as follows (Figure 8): (i) upregulation of BMPs expression and increasing BMP signaling, (ii) increasing the levels of GLUT1 and GLUT4, (iii) activating major signaling mechanisms regulating GLUT4 translocation, (iv) decreasing basal and ATP-linked respiration in mitochondria, and (v) sensitizing to insulin in myotubes. All of these changes can contribute to elevated glucose uptake, as demonstrated in the present study by the detection of an increased uptake of the glucose analog  $^{18}\text{F}$ FDG in myoblasts and myotubes, and also the increased  $^{18}\text{F}$ FDG uptake of skeletal muscle, liver, and adipose tissue. Further studies are necessary to elucidate the precise molecular mechanism of tilorone action and identify novel target genes besides BMPs. Since the BMP pathway is a promising drug target for the treatment of insulin resistance and DM it would also be required to test the potential therapeutic effect of tilorone in case of these diseases, as well as in skeletal muscle diseases in which BMP signaling is disturbed. Our study may expand the use of tilorone, which is already in the market.

#### ACKNOWLEDGMENTS

The authors thank Erzsebet Radi and Zita Makrane Felho (University of Szeged) for their excellent technical assistance. Authors wish to thank to Scanomed Ltd. (Scanomed Translational Centre, Debrecen, Hungary) for the in vivo imaging. This research was supported by the National Research, Development and Innovation Office of Hungary [grant numbers: GINOP-2.3.2-15-2016-00040 (MYOTeam), EFOP-

3.6.2-16-2017-00006, NKFI FK 134684, and NKFI K 132446]. Project no. TKP2021-EGA-28 has been implemented with the support provided by the Ministry of Innovation and Technology of Hungary from the National Research, Development and Innovation Fund, financed under the TKP2021-EGA funding scheme. The work was further supported by the János Bolyai Research Scholarship of the Hungarian Academy of Sciences (to A. K.-P.), UNKP-21-5-SZTE-571 New National Excellence Program of the Ministry for Innovation and Technology Sciences (to A. K.-P.), and University of Szeged Open Access Fund (grant number: 6150).

#### CONFLICT OF INTEREST STATEMENT

The authors declare no conflict of interest.

#### ORCID

Zoltan M. Kohler  <http://orcid.org/0000-0002-8299-105X>

Aniko Keller-Pinter  <http://orcid.org/0000-0002-4105-8458>

#### REFERENCES

- Armoni, M., Harel, C., & Karnieli, E. (2007). Transcriptional regulation of the GLUT4 gene: From PPAR-gamma and FOXO1 to FFA and inflammation. *Trends in Endocrinology and Metabolism: TEM*, 18(3), 100–107. <https://doi.org/10.1016/j.TEM.2007.02.001>
- Chattopadhyay, T., Singh, R. R., Gupta, S., & Surolia, A. (2017). Bone morphogenetic protein-7 (BMP-7) augments insulin sensitivity in mice with type II diabetes mellitus by potentiating PI3K/AKT pathway: BMP-7 potentiates insulin signaling, enhances glucose uptake. *Biofactors*, 43(2), 195–209. <https://doi.org/10.1002/biof.1334>
- DeFronzo, R. A., & Tripathy, D. (2009). Skeletal muscle insulin resistance is the primary defect in type 2 diabetes. *Diabetes Care*, 32(Suppl. 2), S157–S163. <https://doi.org/10.2337/dc09-S302>
- Doerrier, C., Garcia-Souza, L. F., Krumschnabel, G., Wohlfarter, Y., Mészáros, A. T., & Gnaiger, E. (2018). High-resolution Fluorescence Respirometry and OXPHOS protocols for human cells, permeabilized fibers from small biopsies of muscle, and isolated mitochondria. *Mitochondrial Bioenergetics* (pp. 31–70). Springer. [https://doi.org/10.1007/978-1-4939-7831-1\\_3](https://doi.org/10.1007/978-1-4939-7831-1_3)
- Dranka, B. P., Hill, B. G., & Darley-Usmar, V. M. (2010). Mitochondrial reserve capacity in endothelial cells: The impact of nitric oxide and reactive oxygen species. *Free Radical Biology and Medicine*, 48(7), 905–914. <https://doi.org/10.1016/j.freeradbiomed.2010.01.015>
- Duan, Y., Li, F., Wang, W., Guo, Q., Wen, C., & Yin, Y. (2017). Alteration of muscle fiber characteristics and the AMPK-SIRT1-PGC-1 $\alpha$  axis in skeletal muscle of growing pigs fed low-protein diets with varying branched-chain amino acid ratios. *Oncotarget*, 8(63), 107011–107021. <https://doi.org/10.18632/oncotarget.22205>
- Ekins, S., Lingerfelt, M. A., Comer, J. E., Freiberg, A. N., Mirsalis, J. C., O'Loughlin, K., Harutyunyan, A., McFarlane, C., Green, C. E., & Madrid, P. B. (2018). Efficacy of tilorone dihydrochloride against Ebola virus infection. *Antimicrobial Agents and Chemotherapy*, 62(2), e01711–17. <https://doi.org/10.1128/AAC.01711-17>
- Hardie, D. G., Ross, F. A., & Hawley, S. A. (2012). AMPK: A nutrient and energy sensor that maintains energy homeostasis. *Nature Reviews Molecular Cell Biology*, 13(4), 251–262. <https://doi.org/10.1038/nrm3311>
- Holman, N., Young, B., & Gadsby, R. (2015). Current prevalence of Type 1 and Type 2 diabetes in adults and children in the UK. *Diabetic Medicine*, 32(9), 1119–1120. <https://doi.org/10.1111/dme.12791>
- Horlock, D., Kaye, D. M., Winbanks, C. E., Gao, X. M., Kiriazis, H., Donner, D. G., Gregorevic, P., McMullen, J. R., & Bernardo, B. C. (2021). Old drug, new trick: Tilorone, a broad-spectrum antiviral drug as a potential anti-fibrotic therapeutic for the diseased heart. *Pharmaceuticals*, 14(3), 263. <https://doi.org/10.3390/PH14030263>
- Huang, S., & Czech, M. P. (2007). The GLUT4 glucose transporter, 5 *cell metabolism* §. Cell Press. <https://doi.org/10.1016/j.cmet.2007.03.006>
- Ishikura, S., Bilan, P. J., & Klip, A. (2007). Rabs 8A and 14 are targets of the insulin-regulated Rab-GAP AS160 regulating GLUT4 traffic in muscle cells. *Biochemical and Biophysical Research Communications*, 353(4), 1074–1079. <https://doi.org/10.1016/j.bbrc.2006.12.140>
- Jaldin-Fincati, J. R., Pavarotti, M., Frendo-Cumbo, S., Bilan, P. J., & Klip, A. (2017). Update on GLUT4 vesicle traffic: A cornerstone of insulin action. *Trends in Endocrinology and Metabolism: TEM*, 28(8), 597–611. <https://doi.org/10.1016/j.tem.2017.05.002>
- Jamwal, S., Blackburn, J., & Elsworth, J. D. (2020). PPAR $\gamma$ /PGC1 $\alpha$  signaling as a potential therapeutic target for mitochondrial biogenesis in neurodegenerative disorders. *Pharmacology & Therapeutics*, 219, 107705. <https://doi.org/10.1016/j.pharmthera.2020.107705>
- Janani, C., & Ranjitha Kumari, B. D. (2015). PPAR gamma gene—A review. *Diabetes & Metabolic Syndrome*, 9(1), 46–50. <https://doi.org/10.1016/j.dsx.2014.09.015>
- Joost, H.-G., Bell, G. I., Best, J. D., Birnbaum, M. J., Charron, M. J., Chen, Y. T., Doege, H., James, D. E., Lodish, H. F., Moley, K. H., Moley, J. F., Mueckler, M., Rogers, S., Schürmann, A., Seino, S., & Thorens, B. (2002). Nomenclature of the GLUT/SLC2A family of sugar/polyol transport facilitators. *American Journal of Physiology-Endocrinology And Metabolism*, 282(4), E974–E976. <https://doi.org/10.1152/ajpendo.00407.2001>
- Kahn, B. B., & Mcgraw, T. E. (2010). Rosiglitazone, PPAR $\gamma$ , and Type 2 diabetes. *New England Journal of Medicine*, 363, 2667–2669. <https://doi.org/10.1056/NEJMcibr1012075>
- Katz, E., Margalith, E., & Winer, B. (1976). Inhibition of herpesvirus deoxyribonucleic acid and protein synthesis by tilorone hydrochloride. *Antimicrobial Agents and Chemotherapy*, 9(1), 189–195. <https://doi.org/10.1128/AAC.9.1.189>
- Kocsis, T., Baán, J., Müller, G., Mandler, L., Dux, L., & Keller-Pintér, A. (2014). Skeletal muscle cellularity and glycogen distribution in the hypermuscular compact mice. *European Journal of Histochemistry*, 58(3), 169–175. <https://doi.org/10.4081/ejh.2014.2353>
- Krueger, R. F., & Mayer, G. D. (1970). Tilorone hydrochloride: An orally active antiviral agent. *Science*, 169(3951), 1213–1214. <https://doi.org/10.1126/science.169.3951.1213>
- Lane, T. R., & Ekins, S. (2020). Toward the target: Tilorone, quinacrine, and pyronaridine bind to ebola virus glycoprotein. *ACS Medicinal Chemistry Letters*, 11(8), 1653–1658. <https://doi.org/10.1021/acsmchemlett.0c00298>
- Leppäranta, O., Tikkanen, J. M., Bespalov, M. M., Koli, K., & Myllärniemi, M. (2013). Bone morphogenetic protein-inducer tilorone identified by high-throughput screening is antifibrotic in vivo. *American Journal of Respiratory Cell and Molecular Biology*, 48(4), 448–455. <https://doi.org/10.1165/rcmb.2012-0201OC>
- Leto, D., & Saltiel, A. R. (2012). Regulation of glucose transport by insulin: Traffic control of GLUT4. *Nature Reviews Molecular Cell Biology*, 13(6), 383–396. <https://doi.org/10.1038/nrm3351>
- Liang, H., & Ward, W. F. (2006). PGC-1 $\alpha$ : A key regulator of energy metabolism. *Advances in Physiology Education*, 30, 145–151. <https://doi.org/10.1152/advan.00052.2006>
- Loginova, S., Koval'chuk, A. V., Borisevich, S. V., Syromiatnikova, S. I., Borisevich, G. V., Pashchenko, I., Khamitov, R. A., Maksimov, V. A., & Shuster, A. M. (2004). Antiviral activity of an interferon inducer amixin in experimental West Nile Fever. *Voprosy Virusologii*, 49(2), 8–11.

- Mangnall, D., Bruce, C., & Fraser, R. B. (1993). Insulin-stimulated glucose uptake in C2C12 myoblasts. *Biochemical Society Transactions*, 21(4):438S. <https://doi.org/10.1042/BST021438S>
- Massagué, J., Seoane, J., & Wotton, D. (2005). Smad transcription factors. *Genes & Development*, 19(23), 2783–2810. <https://doi.org/10.1101/gad.1350705>
- Modica, S., Straub, L. G., Balaz, M., Sun, W., Varga, L., Stefanicka, P., Profant, M., Simon, E., Neubauer, H., Ukropcova, B., Ukropec, J., & Wolftrum, C. (2016). Bmp4 promotes a brown to white-like adipocyte shift. *Cell Reports*, 16(8), 2243–2258. <https://doi.org/10.1016/j.celrep.2016.07.048>
- Nászai, A., Terhes, E., Kaszaki, J., Boros, M., & Juhász, L. (2019). Ca<sup>2+</sup> N it be measured? Detection of extramitochondrial calcium movement with high-resolution FluoRespirometry. *Scientific Reports*, 9(1), 19229. <https://doi.org/10.1038/s41598-019-55618-5>
- Nishimura, T., Okobira, T., Kelly, A. M., Shimada, N., Takeda, Y., & Sakurai, K. (2007). DNA binding of tilorone: 1H NMR and calorimetric studies of the intercalation. *Biochemistry*, 46(27), 8156–8163. <https://doi.org/10.1021/bi602402m>
- Pauk, M., Bordukalo-Niksic, T., Brkljacic, J., Paralkar, V. M., Brault, A. L., Dumic-Cule, I., Borovecki, F., Grgurevic, L., & Vukicevic, S. (2019). A novel role of bone morphogenetic protein 6 (BMP6) in glucose homeostasis. *Acta Diabetologica*, 56(3), 365–371. <https://doi.org/10.1007/s00592-018-1265-1>
- Puhl, A. C., Fritch, E. J., Lane, T. R., Tse, L. V., Yount, B. L., Sacramento, C. Q., Fintelman-Rodrigues, N., Tavella, T. A., Maranhão Costa, F. T., Weston, S., Logue, J., Frieman, M., Premkumar, L., Pearce, K. H., Hurst, B. L., Andrade, C. H., Levi, J. A., Johnson, N. J., Kisthardt, S. C., ... Ekins, S. (2021). Repurposing the ebola and marburg virus inhibitors tilorone, quinacrine, and pyronaridine: In vitro activity against SARS-CoV-2 and potential mechanisms. *ACS Omega*, 6(11), 7454–7468. <https://doi.org/10.1021/acsomega.0c05996>
- Qian, S.-W., Tang, Y., Li, X., Liu, Y., Zhang, Y.-Y., Huang, H.-Y., Xue, R. D., Yu, H. Y., Guo, L., Gao, H. D., Liu, Y., Sun, X., Li, Y. M., Jia, W. P., & Tang, Q. Q. (2013). BMP4-mediated brown fat-like changes in white adipose tissue alter glucose and energy homeostasis. *Proceedings of the National Academy of Sciences*, 110(9), E798–E807. <https://doi.org/10.1073/pnas.1215236110>
- Ratan, R. R., Siddiq, A., Aminova, L., Langley, B., McConoughey, S., Karpisheva, K., Lee, H. H., Carmichael, T., Kornblum, H., Coppola, G., Geschwind, D. H., Hoke, A., Smirnova, N., Rink, C., Roy, S., Sen, C., Beattie, M. S., Hart, R. P., Grumet, M., ... Gazaryan, I. (2008). Small molecule activation of adaptive gene expression: Tilorone or its analogs are novel potent activators of hypoxia inducible factor-1 that provide prophylaxis against stroke and spinal cord injury. *Annals of the New York Academy of Sciences*, 1147(1), 383–394. <https://doi.org/10.1196/annals.1427.033>
- Rauch, C., & Loughna, P. (2005). C2C12 skeletal muscle cells exposure to phosphatidylcholine triggers IGF-1 like-responses. *Cellular Physiology and Biochemistry*, 15(5), 211–224. <https://doi.org/10.1159/000086408>
- Reaven, G. M. (1988). Role of insulin resistance in human disease. *Diabetes*, 37(12), 1595–1607. <https://doi.org/10.2337/diab.37.12.1595>
- Saeedi, P., Petersohn, I., Salpea, P., Malanda, B., Karuranga, S., Unwin, N., Colagiuri, S., Guariguata, L., Motala, A. A., Ogurtsova, K., Shaw, J. E., Bright, D., & Williams, R. (2019). Global and regional diabetes prevalence estimates for 2019 and projections for 2030 and 2045: Results from the International Diabetes Federation Diabetes Atlas, 9th edition. *Diabetes Research and Clinical Practice*, 157, 107843. <https://doi.org/10.1016/j.diabres.2019.107843>
- Sartori, R., Hagg, A., Zampieri, S., Armani, A., Winbanks, C. E., Viana, L. R., Haidar, M., Watt, K. I., Qian, H., Pezzini, C., Zanganeh, P., Turner, B. J., Larsson, A., Zanchettin, G., Pierobon, E. S., Moletta, L., Valmasoni, M., Ponzoni, A., Attar, S., ... Sandri, M. (2021). Perturbed BMP signaling and denervation promote muscle wasting in cancer cachexia. *Science Translational Medicine*, 13(605), eaay9592. <https://doi.org/10.1126/scitranslmed.aay9592>
- Sartori, R., Schirwis, E., Blaauw, B., Bortolanza, S., Zhao, J., Enzo, E., Stantzou, A., Mouisel, E., Toniolo, L., Ferry, A., Stricker, S., Goldberg, A. L., Dupont, S., Piccolo, S., Amthor, H., & Sandri, M. (2013). BMP signaling controls muscle mass. *Nature Genetics*, 45(11), 1309–1318. <https://doi.org/10.1038/ng.2772>
- Schreiber, I., Dörpholz, G., Ott, C. E., Kragesteen, B., Schanze, N., Lee, C. T., Köhrle, J., Mundlos, S., Ruschke, K., & Knaus, P. (2017). BMPs as new insulin sensitizers: Enhanced glucose uptake in mature 3T3-L1 adipocytes via PPAR $\gamma$  and GLUT4 upregulation. *Scientific Reports*, 7(1), 17192. <https://doi.org/10.1038/s41598-017-17595-5>
- Shen, L., Niu, J., Wang, C., Huang, B., Wang, W., Zhu, N., Deng, Y., Wang, H., Ye, F., Cen, S., & Tan, W. (2019). High-throughput screening and identification of potent broad-spectrum inhibitors of coronaviruses. *Journal of Virology*, 93(12), e00023-19. <https://doi.org/10.1128/JVI.00023-19>
- Sun, Y., Bilan, P. J., Liu, Z., & Klip, A. (2010). Rab8A and Rab13 are activated by insulin and regulate GLUT4 translocation in muscle cells. *Proceedings of the National Academy of Sciences*, 107(46), 19909–19914. <https://doi.org/10.1073/pnas.1009523107>
- Townsend, K. L., An, D., Lynes, M. D., Huang, T. L., Zhang, H., Goodyear, L. J., & Tseng, Y.-H. (2013). Increased mitochondrial activity in BMP7-treated brown adipocytes, due to increased CPT1-and CD36-mediated fatty acid uptake. *Antioxidants & Redox Signaling*, 19(3), 243–257. <https://doi.org/10.1089/ars.2012.4536>
- Tulipano, G., Spano, P., & Cocchi, D. (2008). Effects of olanzapine on glucose transport, proliferation and survival in C2C12 myoblasts. *Molecular and Cellular Endocrinology*, 292(1–2), 42–49. <https://doi.org/10.1016/j.mce.2008.04.010>
- Wang, C., Silverman, R. M., Shen, J., & O'Keefe, R. J. (2018). Distinct metabolic programs induced by TGF- $\beta$ 1 and BMP2 in human articular chondrocytes with osteoarthritis. *Journal of Orthopaedic Translation*, 12, 66–73. <https://doi.org/10.1016/j.jot.2017.12.004>
- Wang, D., Jiang, X., Lu, A., Tu, M., Huang, W., & Huang, P. (2018). BMP14 induces tenogenic differentiation of bone marrow mesenchymal stem cells in vitro. *Experimental and Therapeutic Medicine*, 16(2), 1165–1174. <https://doi.org/10.3892/etm.2018.6293>
- Wong, C. Y., Al-Salami, H., & Dass, C. R. (2020). C2C12 cell model: Its role in understanding of insulin resistance at the molecular level and pharmaceutical development at the preclinical stage. *Journal of Pharmacy and Pharmacology*, 72(12), 1667–1693. <https://doi.org/10.1111/jphp.13359>
- Won, J. C. (2021). Thiazolidinediones (TZDs), In S. H. Lee & D. W. Kang (Eds.), *Stroke revisited: Diabetes in stroke*. Springer. [https://doi.org/10.1007/978-981-16-5123-6\\_11](https://doi.org/10.1007/978-981-16-5123-6_11)
- Wu, Z., Xie, Y., Morrison, R. F., Bucher, N. L., & Farmer, S. R. (1998). PPARgamma induces the insulin-dependent glucose transporter GLUT4 in the absence of C/EBPalpha during the conversion of 3T3 fibroblasts into adipocytes. *Journal of Clinical Investigation*, 101(1), 22–32. <https://doi.org/10.1172/JCI1244>
- Yu, Y., Mutlu, A. S., Liu, H., & Wang, M. C. (2017). High-throughput screens using photo-highlighting discover BMP signaling in mitochondrial lipid oxidation. *Nature Communications*, 8(1), 865. <https://doi.org/10.1038/s41467-017-00944-3>
- Zhao, F.-Q., & Keating, A. (2007). Functional properties and genomics of glucose transporters. *Current Genomics*, 8(2), 113–128. <https://doi.org/10.2174/138920207780368187>
- Zhou, G., Myers, R., Li, Y., Chen, Y., Shen, X., Fenyk-Melody, J., Wu, M., Ventre, J., Doebber, T., Fujii, N., Musi, N., Hirshman, M. F., Goodyear, L. J., & Moller, D. E. (2001). Role

- of AMP-activated protein kinase in mechanism of metformin action. *Journal of Clinical Investigation*, 108(8), 1167–1174. <https://doi.org/10.1172/JCI13505>
- Zimmet, P., Alberti, K. G. M. M., & Shaw, J. (2001). Global and societal implications of the diabetes epidemic. *Nature*, 414(6865), 782–787. <https://doi.org/10.1038/414782a>
- Zorzano, A., Fandos, C., & Palacin, M. (2000). Role of plasma membrane transporters in muscle metabolism. *Biochemical Journal*, 349(3), 667–688. <https://doi.org/10.1042/BJ3490667>

**How to cite this article:** Kohler, Z. M., Trencsenyi, G., Juhasz, L., Zvara, A., Szabo, J. P., Dux, L., Puskas, L. G., Rovo, L., & Keller-Pinter, A. (2023). Tilorone increases glucose uptake in vivo and in skeletal muscle cells by enhancing Akt2/AS160 signaling and glucose transporter levels. *Journal of Cellular Physiology*, 238, 1080–1094. <https://doi.org/10.1002/jcp.30998>